Journal of Energy Chemistry 30 (2019) 42–48

Contents lists available at ScienceDirect

Journal of Energy Chemistry

journal homepage: www.elsevier.com/locate/jechem

http://www.journals.elsevier.com/journal-of-energy-chemistry/

The effect of oxidation of ethane to oxygenates on Pt- and Zn-containing LTA zeolites with tunable selectivity

Baoyu Liu[a,*], Su Cheun Oh[b], Huiyong Chen[c], Dongxia Liu[b,*]

[a] School of Chemical Engineering and Light Industry, Guangdong University of Technology, Guangzhou 510640, Guangdong, China
[b] Department of Chemical and Biomolecular Engineering, University of Maryland, College Park, Maryland 20742, United States
[c] School of Chemical Engineering, Northwest University, Xi'an 710069, Shaanxi, China

ARTICLE INFO

Article history:
Received 26 January 2018
Revised 28 March 2018
Accepted 1 April 2018
Available online 5 April 2018

Keywords:
Zeolite
Hierarchical
Ethane
Porosity

ABSTRACT

Platinum and zinc containing LTA zeolite catalysts with tunable meso/microporosity were prepared by using ligand-metal precursors under hydrothermal condition. These materials were employed for oxidation of ethane to oxygenates using hydrogen peroxides as oxidant under mild reaction condition. The results showed that platinum and zinc loaded LTA zeolites were effective for the partial oxidation of ethane with hydrogen peroxide giving the desired C_2 oxygenates. Moreover, the C_1 oxygenates were also obtained through subsequent C–C bond scission pathways. The over oxidation of ethanol/methanol to acetic acid/formic acid could be inhibited through the introduction of mesoporosity in LTA zeolites. Our findings for oxidation of ethane suggested that the selectivity to the oxidation products such as alcohols and acids could be tailored by tuning the metal species within the LTA zeolites and porosity of catalysts, indicating that a balance between the meso/microporosity and metal species in LTA zeolites can be realized for desirable catalysis by one-pot synthesis of zeolites. In addition, the selectivity to oxygenates can also be tuned by control of the reaction conditions, i.e. concentration of hydrogen peroxide or reaction time.

1. Introduction

The depletion of fossil fuels has stimulated scientists to explore alternative type of fuels to substitute fossil fuel as feedstocks for various chemicals production. Natural gas, which is estimated to have more than 190 trillion cubic meters [1], is an abundant resource that is composed mainly of methane (70%–90%) and ethane (1%–10%). Thus, it is necessary to convert natural gas to valuable chemicals and fuels. In the past few decades, intensive research has focused on methane conversion processes to higher hydrocarbons. For example, the hydrocarbons can be obtained through steam reforming of methane to produce syngas (CO and H_2) followed by consecutive Fischer–Tropsch synthesis [2,3]. Besides, direct methane aromatization to aromatics (DMA) and oxidative coupling of methane to C_2 products have also been deeply investigated [4–7]. However, the high C–H bond strength (439.57 kJ/mol) of CH_4 makes the processes relatively unfavorable since energy intensive steps are involved [8].

Ethane, another main constituent of natural gas, has lower C–H strength of 423.29 kJ/mol and higher solubility in water than methane [9]. Ethane is wieldy used to produce light olefins through steam cracking on zeolite catalyst. However, steam cracking process requires plenty of energy. Therefore, partial oxidation of ethane to value-added products is an alternative approach to circumvent energy intensive processes. Considerable efforts have been made to convert ethane to valuable chemicals and fuels through partial oxidation of ethane. Thorsteinson et al. [10] has reported that Mo/V/Nb catalysts were able to activate ethane by using O_2 and air, and the ethane could be converted to ethene, acetic acid and CO_x, at reaction temperature of 423–723 K. On the other hand, Moffat. [11] discovered that no acetic acid was found when ethane conversion reaction was run at 813 K using silica loaded HPMo catalyst. Vanadium oxide containing silica catalysts exhibited low ethane conversion (3%), but high acetaldehyde selectivity (45%) [12]. High ethane conversion (73%) and ethene selectivity (83%) can be achieved by using alumina supported Pt–Sn catalyst [13], but these approaches need to be carried out under high temperature and pressure conditions.

Shul'pin et al. [14,15] used iron (III) species as catalysts for ethane conversion reactions in H_2O_2 or acetonitrile media activation and the results showed that high selectivity to ethylhydroperoxide (88%) with ethanol (3%) products could be obtained. The superior performance could be attributed to the fessyl species formed by the interaction between H_2O_2 and hydroperoxy radicals (·OOH). However, the drawback of this system involves homogeneous catalysis that is unfavorable for chemical separation.

* Corresponding authors.
E-mail addresses: baoyu.liu@gdut.edu.cn (B. Liu), liud@umd.edu (D. Liu).

https://doi.org/10.1016/j.jechem.2018.04.001

Table 1. Weight percentages of compositions in synthesis gel of metal containing LTA zeolites.

Samples	Metal precursor used	Content of metal precursor (wt%)	Content (wt%)				
			Na_2O	Al_2O_3	SiO_2	H_2O	TPOAC
M-LTA-Pt	$[Pt(NH_3)_4](NO_3)_2$	0.1	7.8	5.3	4.4	82.4	0.0
M-LTA-Zn	$Zn(C_5H_7O_2)_2 \cdot H_2O$	0.3	7.8	5.3	4.4	82.2	0.0
H-LTA-Pt	$[Pt(NH_3)_4](NO_3)_2$	0.1	7.6	5.1	4.3	80.0	2.9
H-LTA-Zn	$Zn(C_5H_7O_2)_2 \cdot H_2O$	0.3	7.6	5.1	4.3	79.8	2.9
H-LTA-Pt@Zn	$[Pt(NH_3)_4](NO_3)_2$	0.1	7.6	5.1	4.3	79.8	2.9
	$Zn(C_5H_7O_2)_2 \cdot H_2O$	0.2					

Meinhold et al. [16] and Kawakami et al. [17] reported that variants of P450 BM3 was active for direct oxidation of ethane to ethanol using O_2 under mild conditions. The results showed that the TOF of the reaction was 500 $mol_{ethanol} \cdot mol_{protein}^{-1} \cdot h^{-1}$. Unfortunately, these enzymatic methods have not been implemented owing to the complexity of enzymes [9]. A biomimetic approach for oxidation of ethane was reported by Xiao at al. [18] who employed metal organic frameworks with iron species as the catalysts to active ethane under N_2O atmosphere. Experimental results showed that the selectivity of products could be tuned by manipulating the reaction condition such as flow rates and batch operations, but additional side products derived from MOFs was neglected [1].

Despite tremendous efforts on oxidation of ethane reactions, there are only a few reports on selective ethane oxidation by using heterogeneous catalysts under mild reaction condition [9]. In 1992, Lin and Sen [19] reported that Pt or Pd loaded carbon could catalyze ethane to oxygenates under 373 K. Later, partial oxidation of ethane to acetaldehyde and ethanol was performed at 333 K by using TS-1 as catalyst and H_2O_2 as the oxidant [20]. Recently, Hutchings and co-workers [9] reported that Fe and Cu loaded ZSM-5 zeolite catalysts were effective for partial oxidation of ethane to oxygenates at 323 K with 0.5 M H_2O_2 oxidant. Ethylene produced from ethane under low temperature and aqueous phase conditions was reported for the first time in this research work. In addition, acetic acid was discovered under this reaction conditions too. Extending this work, Armstrong et al. [21] investigated the effect of reaction conditions on the selectivity to C_2 oxygenates, and selective oxidation of ethane was performed in a trickle bed reactor in order to avoid over oxidation reaction. Ethylene with high selectivity (38%) was obtained under optimized mild reaction conditions.

In the present work, Pt- and Zn-containing LTA zeolites with different textural properties were systematically investigated as catalysts for partial oxidation of ethane to oxygenates under mild reaction condition. LTA zeolite possesses small pore apertures [22,23] that inhibit coalescence and Ostwald ripening of loaded metal clusters, resulting in the formation of encapsulation of metal clusters within LTA voids [24]. It has been reported that Zn loaded zeolites were effective catalysts in converting light alkanes to valuable chemicals and fuels [25–27]. Besides, Pt is also an active species for oxidation of ethane in aqueous medium [19,28]. Thus, Zn, Pt and Zn-Pt containing LTA zeolites were synthesized to explore the effects of different actives species on the catalytic performances in oxidation of ethane reactions. Moreover, it is crucial that the porosity of zeolites can influence activity and selectivity of catalysts. Herein, the effects of hierarchical porosity of LTA zeolites on the partial oxidation of ethane were also investigated. The understanding of the relationship between catalyst structures and catalytic performances will form the basis for designing catalysts with enhanced ethane conversion under mild condition.

2. Experimental

2.1. Synthesis of metal containing LTA zeolites

Pt- and Zn-containing LTA zeolites were synthesized by using metal precursors with ligands, which can prevent metal cations from precipitation during the hydrothermal crystallization of zeolites [24]. In addition, Hierarchical LTA zeolites were synthesized by adding 3-(trimethoxysilyl)propyl]octadecyldimethylammonium chloride (TPOAC) to traditional LTA zeolite precursor as mesoporous template [29]. The initial weight percentages of components in synthesis gel were shown in Table 1. In a typical synthesis, 1.2 g $NaAlO_2$, 0.94 g NaOH and 0.4 g TPOAC (presence for hierarchal LTA zeolites) were dissolved in 12.4 mL deionized H_2O. After that, 0.64 g fumed SiO_2 was added to this mixture under magnetic stirring condition. The obtained gel was further stirred for 2 h at 333 K. Next, 0.02 g $[Pt(NH_3)_4](NO_3)_2$ or 0.05 g $Zn(C_5H_7O_2)_2 \cdot H_2O$ dissolved in 3 mL deionized H_2O solution was added slowly into the gel. The final mixture was homogenized under vigorous stirring condition for 1 h at 333 K, and the solution was heated to 373 K (15 h) for crystallization under magnetic stirring. After crystallization, solid precipitates were filtered, dried in air, and calcined at 823 K for 6 h to remove organic templates and ligands. The obtained Pt containing or Zn containing hierarchical LTA zeolites are denoted as H-LTA-Pt and H-LTA-Zn. For comparison, conventional LTA zeolite was synthesized by using the same procedure described above except for the absence of TPOAC.

2.2. Characterization

Powder X-ray diffraction (XRD) patterns were performed on a Bruker D8 ADVANCE diffractometer with Cu K_α radiation ($\lambda = 0.15418$ nm) at 40 kV and 40 mA. N_2 adsorption–desorption isotherms were measured using an Autosorb-iQ analyzer at 77 K. Samples were outgassed for 12 h at 523 K prior to measurement. The specific surface area of the samples was calculated based on the adsorption branch of isotherm by using BET equation. Scanning electron micrograph (SEM) images were obtained on Carl Zeiss, ZEISS Ultra 55 at 5.0 kV. The samples were coated with gold layer before measurement. Transmission electron micrographs (TEM) images were recorded using a JEOL JEM-2100 electron microscope at 200 kV. Ultraviolet–visible (UV–vis) spectra were carried out on a Varian Cary UV-500 spectrometer with $BaSO_4$ as the reference. The metal content of metal containing LTA zeolites was determined by inductively coupled plasma optical emission spectroscopy (ICP-OES, Perkin-Elmer 4300 DV).

2.3. Catalyst testing

The partial oxidation of ethane reactions was performed in a stainless-steel autoclave with Teflon liner vessel. The H_2O_2 aqueous solution and a certain amount of catalyst were added into the vessel. After sealing, the autoclave was purged with ethane to ~ 73 psi, and the reactor was further heated to the reaction temperature for 1.0–6.0 h. After the reaction, the resultant solution was analyzed by gas chromatograph (Agilent 7890A GC) equipped with a methyl-siloxane capillary HP-1 column connected to a FID.

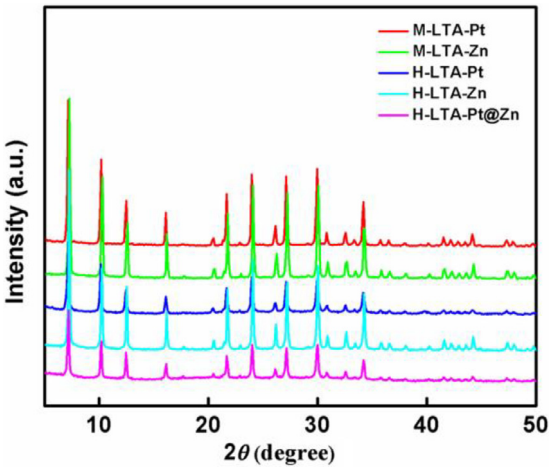

Fig 1. XRD patterns of Pt- and Zn-containing LTA zeolite catalysts.

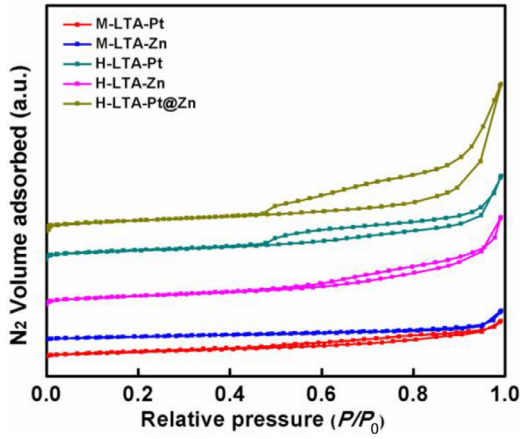

Fig. 2. N_2 adsorption–desorption isotherms of metal containing LTA zeolites.

3. Results and discussion

3.1. Characterization of the metal containing LTA zeolites

The crystalline structure of zeolite catalysts was characterized by XRD, as shown in Fig. 1. All the metal containing zeolite samples exhibited well resolved diffraction peaks, which are typical characteristics of LTA zeolite frameworks [30]. However, the peak intensities of microporous and hierarchical LTA zeolite catalysts are different. With the TPOAC adding into the gel, the diffraction peak intensities of hierarchical LTA zeolites (H-LTA-Pt or H-LTA-Zn) are lower than those of microporous LTA zeolites (M-LTA-Pt or M-LTA-Zn). The possible explanation for this phenomena is that the addition of mesoporous templates into the zeolite frameworks could cause imperfections of LTA single crystals [31]. In addition, there is no significant observation of metal phase for all of the metal loaded LTA zeolites in power XRD patterns, indicating the absence of large metal crystallites in LTA zeolite frameworks [24].

N_2 adsorption–desorption isotherms were employed to determine the porosity features of metal containing LTA zeolites. Fig. 2 shows that M-LTA-Pt and M-LTA-Zn samples exhibit type I isotherm as defined by IUPAC [32], indicating that both M-LTA-Pt and M-LTA-Zn are microporous materials. In contrast, H-LTA-Pt, H-LTA-Zn and H-LTA-Pt@Zn exhibit type-IV isotherms with a hysteresis loop that corresponds to capillary condensation of N_2 in mesopores, verifying that these catalysts consist of both micropores and mesopores structures [33,34]. However, these samples give different hysteresis loops, indicating that they have different hierarchical structures. For H-LTA-Pt and H-LTA-Zn samples, hysteresis loops show a narrow and flat shape, hinting that these materials have slit-like pores [35]. On the other hand, H-LTA-Pt@Zn sample exhibits a broad hysteresis loop, which means that catalyst is composed of wedge-shape pore apertures [32].

Table 2 lists the textural properties of metal loaded LTA zeolites. The BET surface area and total pore volume of M-LTA-Pt/M-LTA-Zn samples are 23 $m^2\ g^{-1}$/12 $m^2\ g^{-1}$ and 0.12 $cm^3\ g^{-1}$/0.10 $cm^3\ g^{-1}$, respectively. The low BET surface area and pore volume indicate that N_2 probe molecules do not easily access the interior of LTA zeolites [36]. With the addition of TPOAC, H-LTA-Pt, H-LTA-Zn and H-LTA-Pt@Zn samples exhibit higher BET surface area and total pore volume than those of M-LTA-Pt and M-LTA-Zn. These data suggests that the extra mesopores originated from TPOAC templates can improve the accessibility of LTA zeolite frameworks, resulting in larger porosity of hierarchical LTA zeolites. Besides, H-LTA-Pt, H-LTA-Zn and H-LTA-Pt@Zn samples show different aperture parameters. For example, the value of mesopore volume and external surface area increase in the order of H-LTA-Pt < H-LTA-Zn < H-LTA-Pt@Zn, but their micropore volumes are the same. These analyses clearly show that the textural properties of metal containing LTA zeolites can be modulated by addition of mesoporous templates and encapsulation of different metal species, which can definitely influence the catalytic properties of the catalysts.

The morphology of metal loaded LTA zeolites was analyzed by SEM. Fig. 3 shows the representative SEM images of micorporous and hierarchical LTA zeolites with different metal species. As shown in Fig. 3(a and b), M-LTA-Pt and M-LTA-Zn exhibit cubic morphology with smooth surface and truncated edges. However, the hierarchically structured LTA zeolites give different morphologies. With the addition of TPOAC to the zeolite synthesis gel, as shown by H-LTA-Pt and H-LTA-Zn in Fig. 3(c and d) respectively, the zeolite morphologies were transformed into sphere-like shape with rough surface. This phenomenon indicates that mesoporous templates could influence the structure of LTA zeolite crystals. Moreover, when both Pt and Zn are loaded into LTA zeolites (H-LTA-Pt@Zn in Fig. 3e), the zeolite composes of numerous domains with nanocrystal morphology. These observations reveal that addition of mesoporous templates and different metal species can influence the morphology of LTA zeolites.

TEM was further conducted to examine the framework structure of resulted metal containing LTA zeolites. Fig. 4(a and b) shows that M-LTA-Pt and M-LTA-Zn consist of plate-like morphology, and the corresponding metal oxide nanoparticles that were encapsulated in the frameworks of LTA zeolites can be observed. H-LTA-Pt and H-LTA-Zn samples shown in Fig. 4(c and d), however, exhibit nanosponge-like structure. Besides, the mesoporous channels in the samples can be easily observed, indicating that H-LTA-Pt and H-LTA-Zn catalysts have open hierarchical microporosity and mesoporosity. Moreover, the relevant metal clusters are dispersed in the isolated form within the LTA crystals, indicating that all of these metals were encapsulated with high dispersion within crystalline NaA frameworks. Fig. 4(e) reveals that dual metals species with small sizes are loaded into frameworks of H-LTA-Pt@Zn catalyst, which is in agreement with XRD results.

The nature of metal species within LTA zeolites was investigated by UV–vis spectroscopy. Fig. 5 shows UV–vis spectra of metal containing LTA zeolites. H-LTA-Pt sample shows an absorption peak at 260 nm, which is assigned to the clusters of Pt nanoparticles [37]. For M-LTA-Pt and H-LTA-Pt@Zn samples, the absorption peak at 260 nm is not observed, indicating the absence of Pt cluster species in M-LTA-Pt and H-LTA-Pt@Zn samples. In addition, the UV–vis spectra of M-LTA-Pt, M-LTA-Pt and H-LTA-Pt@Zn samples shown in Fig. 5 exhibit two absorption peaks in the range from 325 to 350 nm and at about 425 nm, respectively. Pt species in

Table 2. Textural property and details of metal loaded LTA zeolites used in this work.

Sample	S^{a}_{BET} (m^2 g^{-1})	S^{b}_{mic} (m^2 g^{-1})	S^{d}_{ext} (m^2 g^{-1})	V^{c}_{tot} (cm^3 g^{-1})	V^{b}_{mic} (cm^3 g^{-1})	V^{e}_{meso} (cm^3 g^{-1})	Metal loading[f] (wt%)
M-LTA-Pt	23	7	16	0.12	0.01	0.11	0.53
M-LTA-Zn	12	2	10	0.10	0.01	0.09	0.08
H-LTA-Pt	52	21	31	0.28	0.03	0.25	0.56
H-LTA-Zn	60	27	33	0.30	0.03	0.27	0.13
H-LTA-Pt@Zn	52	5	46	0.48	0.03	0.46	Pt 0.19, Zn 0.04

[a] Surface area by Brunauer–Emmett–Teller (BET) method;
[b] Determined from *t*-plot method;
[c] Total pore volumes is obtained at $P/P_0 = 0.95$;
[d] $S_{ext} = S_{BET} - S_{mic}$;
[e] $V_{meso} = V_{total} - V_{mic}$;
[f] Determined from elemental analysis (ICP-OES).

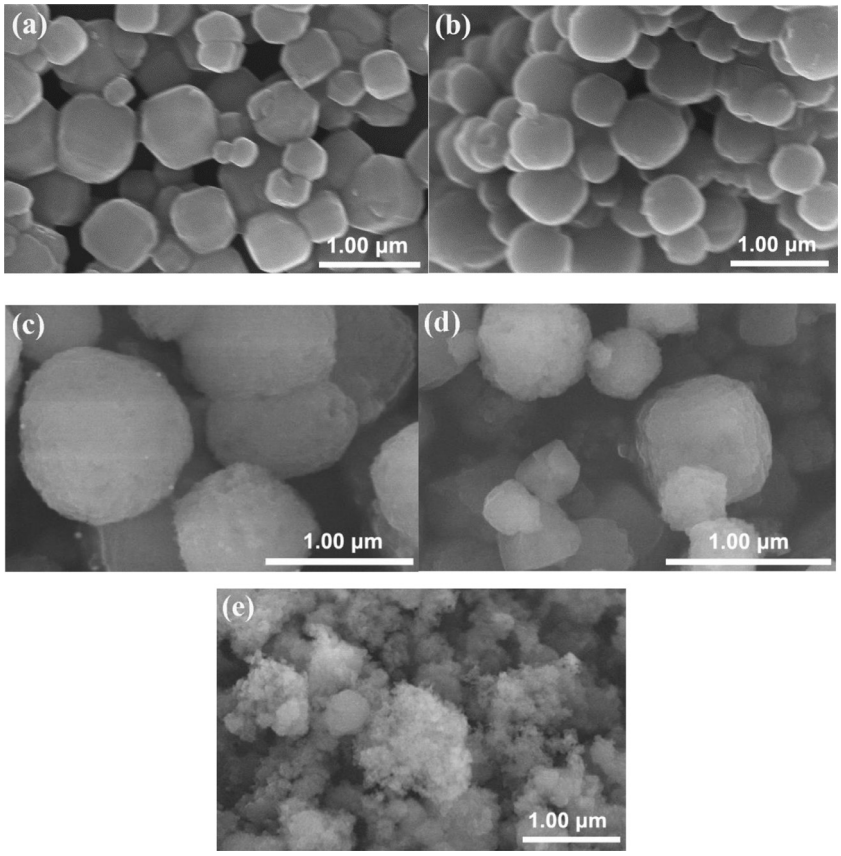

Fig. 3. SEM images showing morphology of (a) M-LTA-Pt, (b) M-LTA-Zn, (c) H-LTA-Pt, (d) H-LTA-Zn and (e) H-LTA-Pt@Zn samples, respectively.

UV–vis bands between 325–350 nm represents the presence of a large number of superficial Pt (IV) complexes that are not easy to be distinguished [38,39], and the band near 425 nm is the characteristic band of bulk platinum (IV) oxides [40]. For M-LTA-Zn, H-LTA-Zn and H-LTA-Pt@Zn samples, absorption peak at ~370 nm that corresponds to ZnO in framework positions was observed [41]. UV–vis analysis shows that metal species exist in LTA zeolite frameworks with different speciation groups.

3.2. Catalytic activity

The metal containing LTA zeolites were employed as heterogeneous catalysts to evaluate the catalytic properties of partial oxidation of ethane under mild reaction condition. Corresponding experimental results are summarized in Fig. 6. The major product obtained from M-LTA-Pt catalyst was methanol while the main product formed from H-LTA-Pt was acetic acid. On the other hand, no formic acid and acetic acid products were observed for M-LTA-Pt catalyst, indicating that the acid products can be expedited by introducing the additional mesoporous in Pt containing LTA zeolites. For M-LTA-Zn and H-LTA-Zn, microporosity was beneficial for the formation of formic acid while mesoporosity inhibited formation of acids. These results reveal that the porosity of LTA zeolites and metal species within LTA zeolite framework can influence the products selectivity in oxidation of ethane reaction.

By changing the metal species, the product distributions can be modulated. For M-LTA-Pt sample, the major product was methanol, which was different from previous reports that ethanol was the primary product when platinum loaded carbon catalyst was used in oxidation of ethane under low temperature [19]. The possible explanation is that kinetic diameter of methanol is ~0.38 nm which matches with the pore size of LTA zeolite (~0.41 nm), and therefore resulted in the formation of methanol. However, formic acid was the primary product with M-LTA-Zn catalyst. This phenomena hints that zinc species in LTA zeolite facilitated further oxidation of methanol to formic acid. Both alcohols and acid products were obtained in H-LTA-Pt catalyst, owing to the unique platinum clusters formed in the zeolite structure. No acid

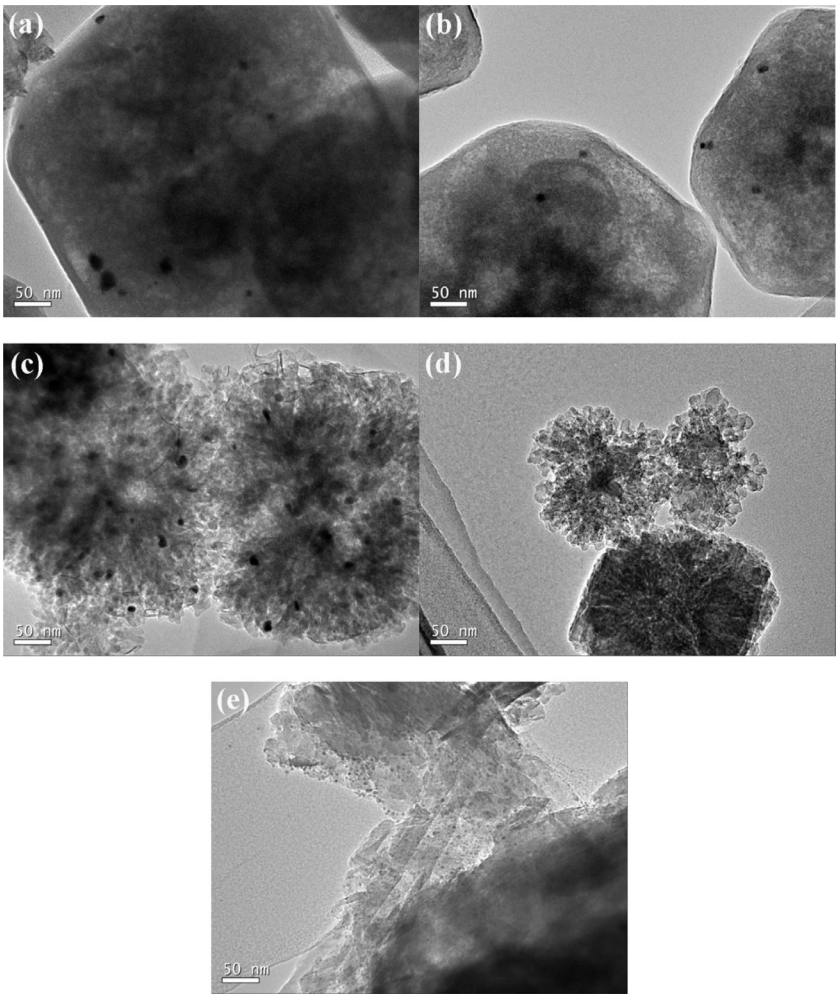

Fig. 4. TEM images of (a) M-LTA-Pt, (b) M-LTA-Zn, (c) H-LTA-Pt, (d) H-LTA-Zn and (e) H-LTA-Pt@Zn samples, respectively.

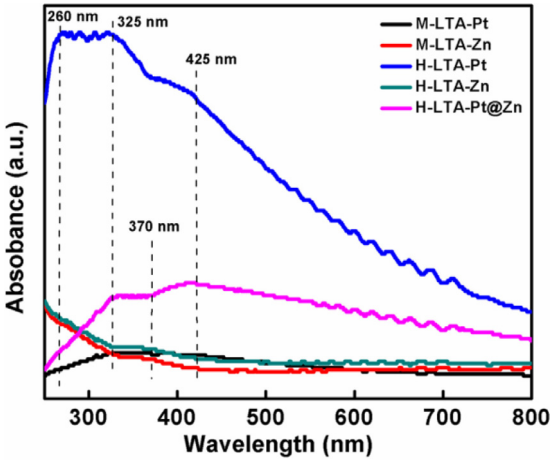

Fig. 5. UV–vis absorbance spectra of Pt- and/or Zn-containing LTA zeolite catalysts.

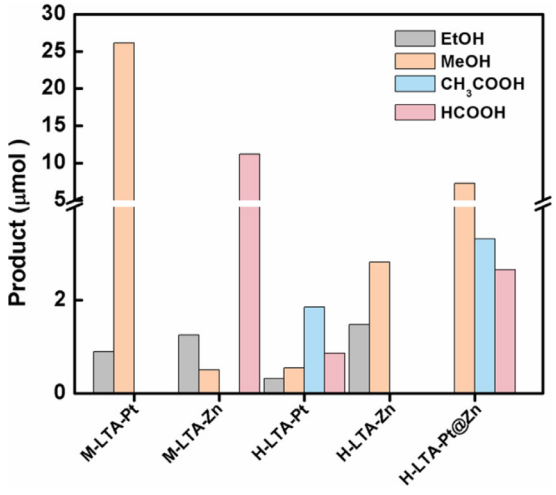

Fig. 6. Distribution of oxygenates in the oxidation of ethane over metal containing LTA zeolites. (Test conditions: 0.06 g catalyst, 10 mL reaction volume, $[H_2O_2]$ 1.0 M, reaction time 1.0 h, $P(C_2H_6) = \sim 73$ psi, $T_{rxn} = 323$ K).

products were formed from H-LTA-Zn catalyst because the presence of mesoporosity in this zeolite improved the mass transport of guest molecules, thus inhibiting the over-oxidation of alcohols. In addition, the bimetallic H-LTA-Pt@Zn sample exhibited high selectivity to methanol (55%) with no ethanol observed, and this can be attributed to the synergistic effect between platinum and zinc metal species.

On the analysis present above, the loaded metal species and porosity of zeolites can influence the distribution of oxygenates simultaneously. The single ZnO species could cause the overoxidation of alcohols, while the three speciation groups for Pt (platinum clusters, superficial Pt (IV) complexes and platinum (IV) oxides) are

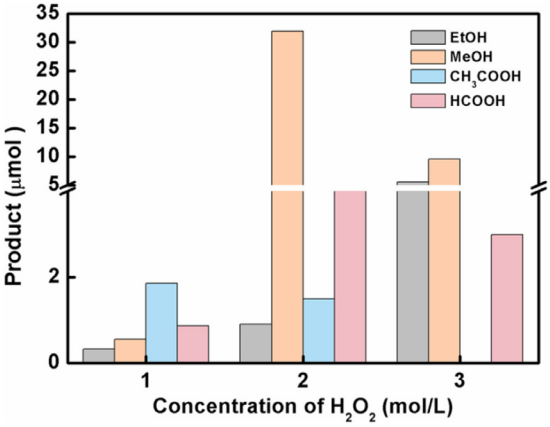

Fig. 7. Effect of H_2O_2 concentration on product selectivities to oxygenates in ethane oxidation over H-LTA-Pt catalyst (Test conditions: 0.06 g catalyst, 10 mL reaction volume, reaction time 1.0 h, $P(C_2H_6)$ = ~73 psi, T_{rxn} = 323 K).

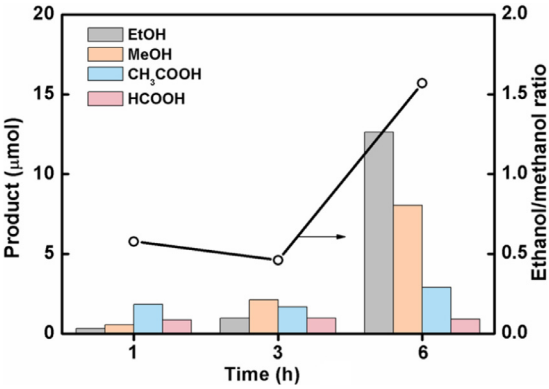

Fig. 8. Effect of reaction time on product selectivities to oxygenates in ethane oxidation over H-LTA-Pt catalyst (Test conditions: 0.06 g catalyst, 10 mL reaction volume, $[H_2O_2]$ 1.0 M, $P(C_2H_6)$ = ~73 psi, T_{rxn} = 323 K).

responsible for activation of C–C and C–H bonds. However, without accurate quantified data for metal species, it is impossible to correlate the catalytic performance with metal species. In addition, the textural property of zeolites can also contribute to the selectivity of oxygenates. For Zn containing LTA zeolites, the increased external surface and mesorporous volume (S_{ext} 33 versus 10 $m^2\ g^{-1}$ and V_{meso} 0.27 versus 0.09 $cm^3\ g^{-1}$) can inhibit the oxidation of alcohols. For Pt containing LTA zeolites, the H-LTA-Pt catalyst produced the various oxygenates due to enhanced accessibility derived from the additional mesoporous compared with M-LTA-Pt (S_{ext} 31 versus 16 $m^2\ g^{-1}$ and V_{meso} 0.25 versus 0.11 $cm^3\ g^{-1}$). The synergy effect of bimetallic M-LTA-Pt@Zn is different from monometallic catalysts, and further detailed studies of the catalysts by in situ techniques are under way in our laboratory.

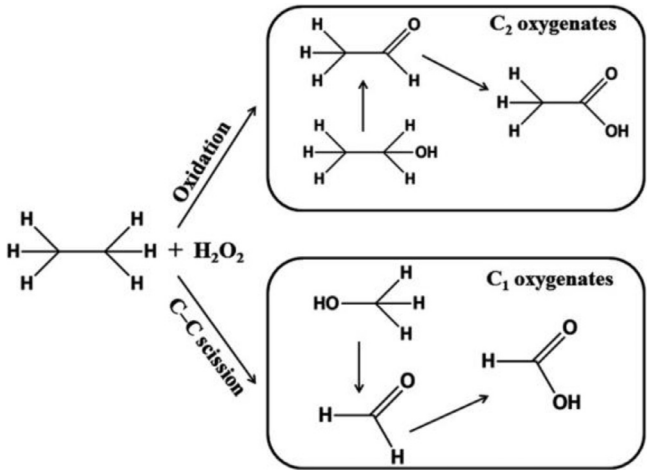

Scheme 1. Proposed reaction network for the oxidation of ethane over Pt- and Zn-containing LTA zeolites in the aqueous phase with H_2O_2 as the oxidant.

The effect of H_2O_2 concentration on the products selectivity was investigated based on the H-LTA-Pt sample, and the results are shown in Fig. 7. It can be noted that the catalyst productivity improved with increasing hydrogen peroxide concentration. When H_2O_2 concentration was 1 M, acetic acid was the major product. When the concentration of hydrogen peroxide reached 2 M, methanol became the major product, followed by formic acid. High H_2O_2 concentration tends to break the C–C bond, resulting in the formation of C_1 oxygenates [9]. However, the main products were methanol and ethanol without acetic acid when the concentration of H_2O_2 was 3 M. Besides, the methanol selectivity showed a volcano-trend dependence on the concentration of hydrogen peroxide, suggesting that tailoring the concentration of hydrogen peroxide could lead to tunable catalytic performances. For comparison, the partial oxidation of ethane was carried out in the absence of hydrogen peroxide, and reaction mixture without additional hydrogen peroxide showed no oxygenates under the investigated reaction condition. This observation clearly demonstrates that hydrogen peroxide is necessary as an oxidant for the partial oxidation of ethane to oxygenates.

The influence of reaction time on products selectivity was also investigated based on the H-LTA-Pt sample, and the results are shown in Fig. 8. Acetic acid was the main product at time on stream of 1 h. When the reaction time was extended to 3 h, product selectivity slightly moved from acetic acid to methanol. The shift in product selectivity might be due to the C–C scission pathways in acetic acid [21]. Nevertheless, the obtained major products were alcohols (methanol and ethanol) when the reaction time was extended to 6 h with highest product selectivity to ethanol (52%). In addition, the ethanol/methanol ratio showed a V-type dependence on the reaction time, indicating that the reaction time should be deliberately optimized in order to improve selectivity to C_2 oxygenates.

Table 3. Product selectivity based on H-LTA-Pt catalyst under optimized reaction conditions.

Entry	Product amount (μmol)				Ethanol/methanol ratio	Reaction conditions
	MeOH	HCOOH	EtOH	CH_3COOH		
1	8.05	0.92	12.63	2.90	1.57	0.06 g catalyst, 10 mL reaction volume, $[H_2O_2]$ 1.0 M, reaction time 6.0 h, $P(C_2H_6)$ = ~73 psi, T_{rxn} = 323 K
2	11.33	2.07	2.31	11.50	0.20	0.12 g catalyst, 20 mL reaction volume, $[H_2O_2]$ 2.0 M, reaction time 6.0 h, $P(C_2H_6)$ = ~73 psi, T_{rxn} = 343 K

The experiment was further carried out under optimized conditions for H-LTA-Pt sample in order to achieve higher selectivity for C_2 oxygenates, and these results were shown in Table 3. It was noted that the low concentration of hydrogen peroxide and long reaction time can improve ethanol/methanol ratio, giving a high selectivity to ethanol. In contrast, with the increasing concentration of hydrogen peroxide, the ethanol selectivity gradually shifted to acetic acid due to deep oxidation reaction, resulting in small ethanol/methanol ratio. The systematic tuning the reaction conditions are necessary to improve the selectivity to C_2 oxygenates.

A possible reaction network for the oxidation of ethane by using Pt- and Zn-containing LTA zeolites as the catalysts under H_2O_2 medium is proposed on the basis of aforementioned analysis and previous literatures [1,9] (Scheme 1). The first catalytic reaction pathway involves the formation of ethanol or ethyl ketone derived from oxidation of ethane, which would further undergo consecutive oxidation to generate acetic acid. The second reaction pathway is related to the C–C bond scission, resulting in the formation of C_1 oxygenates, such as methanol and formic acid due to over oxidation of methanol [19]. In present research, we cannot elucidate the accurate reaction pathway since various parallel and cascade reaction pathways for catalytic oxidation of ethane to oxygenates complicated the reaction network, and the detailed mechanism must await further study. Taking into account our findings, the present proposed reaction network is reasonable on a certain degree.

4. Conclusions

The partial oxidation of ethane to oxygenates was investigated under mild reaction conditions using metal containing LTA zeolites as catalyst. The Pt and Zn encapsulated LTA zeolites were obtained by using ligand-type metal precursors under hydrothermal conditions. In addition, the morphology and porosity of metal containing LTA zeolites were modulated by adding extra TPOAC as mesoporous templates. Moreover, the Pt and Zn containing LTA zeolites exhibited different reaction activities in partial oxidation of ethane to oxygenates under hydrogen peroxide conditions, resulting in distinguished selectivity to C_1 and C_2 oxygenates. Compared to Pt, Zn species were beneficial for formation of formic acid derived from the overoxidation of the C_1 alcohol under the sole presence of microporous LTA zeolite, while the additional mesoporosity could enhance the mass transport of C_1 alcohol, inhibiting the overoxidation of the alcohols. The Pt species were distributed as platinum clusters, superficial Pt (IV) complexes and platinum (IV) oxides in mesoporous Pt containing LTA zeolite, which were responsible for the generation of various oxygenates. Thus, a balance between the metal species and textural properties of LTA zeolites should be deliberately optimized to achieve the desired selectivity to oxygenates. The effect of reaction conditions on products selectivity has also been explored. From our studies, it is clear that the concentration of hydrogen peroxide is a crucial factor to influence product distributions. In addition, the ethanol/methanol ratio can be tuned by changing the reaction time. Hence, our present research work fall into the foundation for future efforts toward designed synthesis of ideal catalysts for direct selective oxidation of ethane to oxygenates under mild reaction conditions.

Acknowledgments

The authors acknowledge the support from the National Science Foundation (NSF-CBET-1264599 and 1351384). We acknowledge the support of the Maryland NanoCenter and its NispLab. The NispLab is supported in part by the NSF as a MRSEC Shared Experimental Facility. Baoyu Liu thanks the China Scholarship Council (CSC) (No. 201306150076) for a fellowship to support his study at the University of Maryland.

References

[1] R. Armstrong, G. Hutchings, S. Taylor, Catalysts 6 (2016) 71.
[2] A. Ghosh, W.E. Holt, Science 335 (2012) 838–843.
[3] X. Chen, D. Deng, X. Pan, Y. Hu, X. Bao, Chem. Commun. 51 (2015) 217–220.
[4] Y. Wu, L. Emdadi, S.C. Oh, M. Sakbodin, D. Liu, J. Catal. 323 (2015) 100–111.
[5] Y. Wu, Z. Lu, L. Emdadi, S.C. Oh, J. Wang, Y. Lei, H. Chen, D.T. Tran, I.C. Lee, D. Liu, J. Catal. 337 (2016) 177–187.
[6] S.C. Oh, Y. Lei, H. Chen, D. Liu, Fuel 191 (2017) 472–485.
[7] S.C. Oh, Y. Wu, D.T. Tran, I.C. Lee, Y. Lei, D. Liu, Fuel 167 (2016) 208–217.
[8] S.J. Blanksby, G.B. Ellison, Acc. Chem. Res. 36 (2003) 255–263.
[9] M.M. Forde, R.D. Armstrong, C. Hammond, Q. He, R.L. Jenkins, S.A. Kondrat, N. Dimitratos, J.A. Lopez-Sanchez, S.H. Taylor, D. Willock, C.J. Kiely, G.J. Hutchings, J. Am. Chem. Soc. 135 (2013) 11087–11099.
[10] E.M. Thorsteinson, T.P. Wilson, F.G. Young, P.H. Kasai, J. Catal. 52 (1978) 116–132.
[11] J.B. Moffat, Appl. Catal. A. 146 (1996) 65–86.
[12] A. Erdöhelyi, F. Solymosi, J. Catal. 129 (1991) 497–510.
[13] A.S. Bodke, D.A. Olschki, L.D. Schmidt, E. Ranzi, Science 285 (1999) 712–715.
[14] G.B. Shul'pin, G.V. Nizova, Y.N. Kozlov, L. Gonzalez Cuervo, G. Süss-Fink, Adv. Synth. Catal. 346 (2004) 317–332.
[15] B. Ensing, F. Buda, P.E. Blochl, E.J. Baerends, Phys. Chem. Chem. Phys. 4 (2002) 3619–3627.
[16] P. Meinhold, M.W. Peters, M.M.Y. Chen, K. Takahashi, F.H. Arnold, ChemBioChem 6 (2005) 1765–1768.
[17] N. Kawakami, O. Shoji, Y. Watanabe, Chem. Sci. 4 (2013) 4532.
[18] D.J. Xiao, E.D. Bloch, J.A. Mason, W.L. Queen, M.R. Hudson, N. Planas, J. Borycz, A.L. Dzubak, P. Verma, K. Lee, F. Bonino, V. Crocellà, J. Yano, S. Bordiga, D.G. Truhlar, L. Gagliardi, C.M. Brown, J.R. Long, Nat. Chem. 6 (2014) 590–595.
[19] M. Lin, A. Sen, J. Am. Chem. Soc. 114 (1992) 7307–7308.
[20] T. Tatsumi, M. Nakamura, S. Negishi, H. Tominaga, ChemInform 21 (1990) 476–477.
[21] R.D. Armstrong, S.J. Freakley, M.M. Forde, V. Peneau, R.L. Jenkins, S.H. Taylor, J.A. Moulijn, D.J. Morgan, G.J. Hutchings, J. Catal. 330 (2015) 84–92.
[22] J. Im, H. Shin, H. Jang, H. Kim, M. Choi, Nat. Commun. 5 (2014) 3370.
[23] K. Cho, H.S. Cho, L.-C. de Ménorval, R. Ryoo, Chem. Mater. 21 (2009) 5664–5673.
[24] Z. Wu, S. Goel, M. Choi, E. Iglesia, J. Catal. 311 (2014) 458–468.
[25] A. Smiešková, E. Rojasová, P. Hudec, L. Šabo, Appl. Catal. A. 268 (2004) 235–240.
[26] J.A. Biscardi, E. Iglesia, Catal. Today 31 (1996) 207–231.
[27] O.A. Anunziata, L.B. Pierella, Catal. Lett. 16 (1992) 437–441.
[28] Q. Yuan, W. Deng, Q. Zhang, Y. Wang, Adv. Synth. Catal. 349 (2007) 1199–1209.
[29] M. Choi, H.S. Cho, R. Srivastava, C. Venkatesan, D.-H. Choi, R. Ryoo, Nat. Mater. 5 (2006) 718–723.
[30] H. Chen, J. Wydra, X. Zhang, P.-S. Lee, Z. Wang, W. Fan, M. Tsapatsis, J. Am. Chem. Soc. 133 (2011) 12390–12393.
[31] Y.C. Feng, Y. Meng, F.X. Li, Z.P. Lv, J.W. Xue, J. Porous Mater. 20 (2013) 465–471.
[32] K.S.W. Sing, D.H. Everett, R.A.W. Haul, L. Moscou, R.A. Pierotti, J. Rouquerol, T. Siemieniewska, Pure Appl. Chem. 57 (1985) 603–619.
[33] B. Liu, Y. Tan, Y. Ren, C. Li, H. Xi, Y. Qian, J. Mater. Chem. 22 (2012) 18631–18638.
[34] B. Liu, K. Xie, S.C. Oh, D. Sun, Y. Fang, H. Xi, Chem. Eng. Sci. 153 (2016) 374–381.
[35] M. Thommes, Chapter 15 – Textural Characterization of Zeolites and Ordered Mesoporous Materials by Physical Adsorption, in: Studies in Surface Science and Catalysis, Elsevier, 2007, p. 495-XIII.
[36] H. Tounsi, S. Mseddi, S. Djemel, Phys. Proc. 2 (2009) 1065–1074.
[37] E. Gharibshahi, E. Saion, Int. J. Mol. Sci. 13 (2012) 14723.
[38] G. Lietz, H. Lieske, H. Spindler, W. Hanke, J. Völter, J. Catal. 81 (1983) 17–25.
[39] H. Lieske, G. Lietz, H. Spindler, J. Völter, J. Catal. 81 (1983) 8–16.
[40] N.S. de Resende, J.-G. Eon, M. Schmal, J. Catal. 183 (1999) 6–13.
[41] A.K. Zak, M.E. Abrishami, W.H.A. Majid, R. Yousefi, S.M. Hosseini, Ceram. Int. 37 (2011) 393–398.